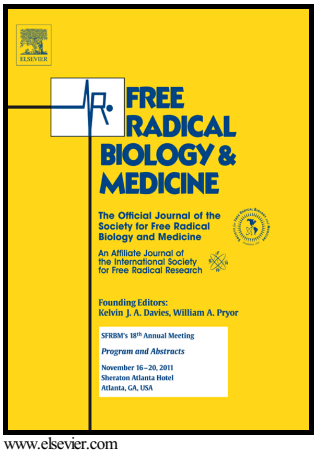

Keto-enol-based modification on piperlongumine to generate a potent Cu(II) ionophore that triggers redox imbalance and death of HepG2 cells

Fang Dai, Cui-Hong Yuan, Yuan Ji, Yu-Ting Du, Xia-Zhen Bao, Ling-Xi Wu, Xiao-Ling Jin, Bo Zhou

PII: S0891-5849(18)30132-1
DOI: https://doi.org/10.1016/j.freeradbiomed.2018.03.029
Reference: FRB13676

To appear in: *Free Radical Biology and Medicine*

Received date: 11 February 2018
Accepted date: 15 March 2018

Cite this article as: Fang Dai, Cui-Hong Yuan, Yuan Ji, Yu-Ting Du, Xia-Zhen Bao, Ling-Xi Wu, Xiao-Ling Jin and Bo Zhou, Keto-enol-based modification on piperlongumine to generate a potent Cu(II) ionophore that triggers redox imbalance and death of HepG2 cells, *Free Radical Biology and Medicine,* https://doi.org/10.1016/j.freeradbiomed.2018.03.029

Keto-enol-based modification on piperlongumine to generate a potent Cu(II) ionophore that triggers redox imbalance and death of HepG2 cells

Fang Dai, Cui-Hong Yuan, Yuan Ji, Yu-Ting Du, Xia-Zhen Bao, Ling-Xi Wu, Xiao-Ling Jin and Bo Zhou*

State Key Laboratory of Applied Organic Chemistry, Lanzhou University, Lanzhou, Gansu 730000, China

*Corresponding author. bozhou@lzu.edu.cn

Abstract

Altered redox status including higher levels of copper in cancer cells than in normal cells inspired many researchers to develop copper ionophores targeting this status. We have recently found that flavon-3-ol (**3-HF**) works as a potent Cu(II) ionophore by virtue of its keto-enol moiety. To further emphasize the significance of this moiety for developing Cu(II) ionophores, we herein designed a β-diketo analog of piperlongumine, **PL-I**, characterized by the presence of high proportion of the keto-enol form in dimethylsulfoxide and chloroform, and identified its keto-enol structure by NMR and theoretical calculations. Benefiting from deprotonation of its enolic hydroxyl group, this molecule is capable of facilitating the transport of Cu(II) through cellular membranes to disrupt redox homeostasis of human hepatoma HepG2 cells and trigger their death.

Graphical Abstract

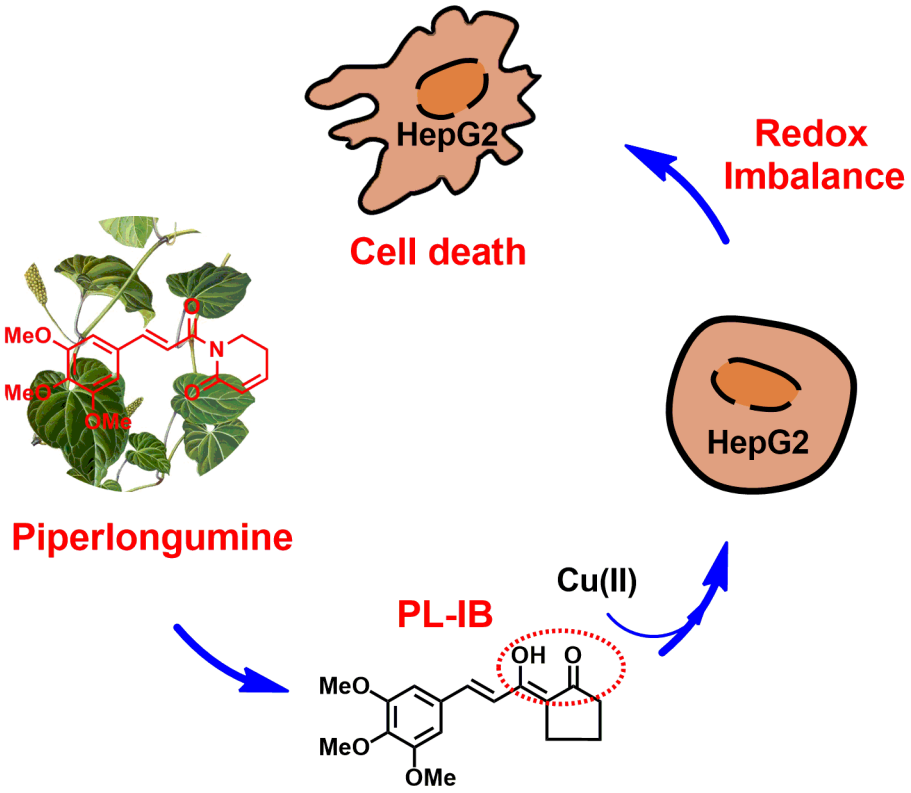

Keywords

Piperlongumine; ionophores; copper; keto-enol, mechanism

1. Introduction

Redox-active copper acts as a catalytic and structural cofactor for enzymes involved in fundamental biological processes [1-3], but its aberrant metabolism has been implicated in a spectrum of human diseases including cancer [4]. For example, many cancer types harbor increased levels of copper which appears to be an essential cofactor for multiple aspects of tumor progression, including growth, angiogenesis and metastasis [5-8]. This realization has prompted the development of copper-based anticancer strategies. The strategies reported to date fall into one of three categories: developing small chemical entities as copper chelators [8,9], copper ionophores [8-11] and copper-trafficking protein inhibitors [12]. Different with traditional copper

chelators that would limit the available copper, copper ionophores rather facilitate the transport of copper ions through lipid bilayers, resulting in copper-dependent death of cancer cells as exemplified by 8-hydroxyquinoline derivatives (including the most studied clioquinol), thiosemicarbazones, disulfiram, elesclomol and pyrazole-pyridine ligands [9-11,13-17].

In this regard, we have recently identified flavon-3-ol (3-hydroxyflavone, **3-HF**) as a potent Cu(II) ionophore [18]. Its 3-hydroxy-4-keto group has also been recognized as a key structural determinant to support its ionophoric role because the acidity (deprotonation of 3-OH) of this group steers the Cu(II) chelation to form a neutral and lipophilic complex (3-HF-Cu) capable of passing through cellular membranes (Scheme 1A) [18]. In the reductive cytoplasm, dissociation of copper from **3-HF-Cu** is facilitated by the reduced glutathione (GSH) in a redox-responsive fashion, leading to collapse of intracellular redox buffering system hallmarked by significant decrease in the ratio of GSH to its disulfide (GSSG) and obvious ROS generation, as well as final apoptosis of human hepatoma HepG2 cells (Scheme 1A) [18]. From this perspective, **3-HF** as a potent Cu(II) ionophore can be viewed as one of prooxidative anticancer agents (PAAs) to trigger redox imbalance and death of cancer cells [18].

3-Hydroxy-4-keto group of **3-HF** is essentially a keto-enol moiety, and inevitably this invites the question: whether is it feasible to develop natural product-inspired Cu(II) ionophores by exploiting this structural moiety? Piperlongumine (**PL**) (piplartine, Scheme 1B), a natural alkaloid isolated from the long pepper (*Piper longum* L.) in 1961 with its correct structure established in 1968 [19], turned out to be

a promising anticancer molecule [20]. This molecule is chemically characterized by the presence of imide functionalities where nitrogen is involved in a cyclic amide and does not bear any proton, precluding the formation of a keto-enol moiety. Considering that β-diketones exist in equilibrium between the diketo and keto-enol forms with the latter being strongly favored by intramolecular hydrogen bond, we thus designed its β-diketo analog, **PL-I** (Scheme 1B), to generate a keto-enol moiety, whilst preserving its trimethoxycinnamoyl part. As part of our effort to develop natural product-inspired PAAs [18,21-25], the present study was conducted to probe (1) whether the designed **PL-I** could work, in a similar fashion to **3-HF**, as a Cu(II) ionophore to facilitate the transport of Cu(II) due to the presence of a keto-enol moiety, and (2) the feasibility to develop natural product-inspired Cu(II) ionophores by exploiting this moiety.

2. Materials and methods

2.1. Materials

Roswell Park Memorial Institute (RPMI)-1640, 3-(4,5-dimethylthiazol-2-yl)-2,5-diphenyltetrazolium bromide (MTT), 2',7'-dichlorofluorescein diacetate (DCFH-DA), yeast glutathione reductase (GR), reduced L-glutathione (GSH), oxidized L-glutathione (GSSG), 5,5'-dithiobis-2-nitrobenzoic acid (DTNB), bathocuproinedisulfonic acid disodium salt (BCDS) and L-buthionine-(S, R)-sulfoximine (BSO) were purchased from Sigma-Aldrich (St. Louis, MO, USA). The NIR fluorescent Cu(I) probe based on the tricarbocyanine fluorophore and the Cu(I) receptor,

bis(2-((2-(ethylthio)ethyl)-thio)ethyl)amine was synthesized according to a previous report [26]. All other chemicals were of analytical grade.

*2.2. Synthesis of **PL-I***

3-(3, 4, 5-Trimethoxyphenyl)propionic acid and its corresponding acyl chloride were synthesized as described previously [27]. To a solution of cyclopentanone (6 mmol) in 15 mL THF at -78℃ was slowly added LDA (6.6 mmol in THF) under dry nitrogen and stirred for 45 min. The acyl chloride (3 mmol) dispersed into 15 mL of THF was added dropwise to the reaction mixture, and the reaction was continued for 1 h at same temperature, and then warmed slowly to room temperature. Reaction mixture was diluted with ethyl acetate, dried with brine and Na_2SO_4, and purified by column chromatograph and recrystallization from ethanol and CH_2Cl_2 to give yellow **PL-I** in 89% yield. **M.p.**: 130-132 ^{o}C; ^{1}H and ^{13}C NMR spectra were recorded on a Bruker AVANCE III 400Hz NMR spectrometer. High resolution mass spectra (HRMS) were measured on a Thermo Scientific Orbitrap Elite mass spectrometer (Concerning ^{1}H NMR, ^{13}C NMR and HRMS spectra of **PL-I**, see also the supplementary data).

PL-IA, **^{1}H-NMR** (400 MHz, DMSO-d_6): 7.58 (d, J = 16.0 Hz, 1H), 7.06 (s, 2H), 6.96 (d, J = 16.0 Hz, 1H), 4.06-4.01(m, 1H), 3.83 (s, 6H), 3.71 (s, 3H), 2.29-2.10 (m, 5H), 2.01-1.97(m, 1H) ppm; **^{13}C NMR** (100 MHz, DMSO-d_6) 214.1, 195.9, 153.1, 144.5, 139.7, 129.9, 125.7, 106.1, 60.1, 58.8, 56.0, 38.5, 26.4, 20.5 ppm; **HRMS** (ESI) m/z calcd for $C_{17}H_{20}O_5$ (M+H): 305.1384. Found: 305.1378, error: 1.6 ppm.

PL-IB, **^{1}H-NMR** (400 MHz, DMSO-d_6): 13.36 (s, 1H), 7.42 (d, *J* = 15.6 Hz, 1H), 7.04 (s, 2H), 6.76 (d, *J* = 15.6 Hz, 1H), 3.83 (s, 6H), 3.70 (s, 3H), 2.76 (t, *J* = 7.2 Hz, 2H), 2.40 (t, *J* = 7.8 Hz, 2H), 1.91 (quin, *J* = 7.4 Hz, 2H) ppm; **^{13}C NMR** (100 MHz, DMSO-d_6): 210.4, 163.1, 153.1, 139.1, 138.8, 130.7, 119.3, 111.2, 105.7, 60.1, 56.0, 37.5, 25.0, 20.2 ppm; **^{1}H-NMR** (400 MHz, $CDCl_3$): 13.34 (s, 1H), 7.46 (d, *J* = 15.6 Hz, 1H), 6.74 (s, 2H), 6.42 (d, *J* = 15.6 Hz, 1H), 3.90 (s, 6H), 3.88 (s, 3H), 2.76 (t, *J* = 7.4 Hz, 2H), 2.46 (t, *J* = 7.8 Hz, 2H), 1.99 (quin, *J* = 7.6 Hz, 2H) ppm; **^{13}C NMR** (100 MHz, $CDCl_3$) 210.4, 163.7, 153.3, 139.5, 139.0, 131.0, 119.0, 110.9, 105.0, 61.0, 56.1, 38.0, 25.5, 20.5 ppm.

2.3. Density functional theory (DFT) calculations

The DFT calculations were performed using the Gaussian09 package [28]. The conformations of different isomers (**PL-IA**, **PL-IB** and **PL-IC**) of **PL-I** were optimized at the B3LYP/6-311G(d,p) level of theory using intergral equation formalism polarized continuum model (IEFCM) to simulate the solvation effect of chloroform, and the default temperature at 298.15 K was used. Vibrational frequency calculations were carried out based on the optimized geometries, and no imaginary frequencies were found for them. Then the two lowest conformations for **PL-IB** and **PL-IC** were used for NMR calculations with the GIAO method.

2.4. UV/Vis spectral measurements

Cu(II)-induced UV/Vis absorption changes of **PL-I** in methanol were monitored at ambient temperature with a TU-1901 UV/Vis spectrophotometer (Beijing Purkinje General Instrument Co., Ltd., Beijing, China). In the case of **PL**, the spectra were run

against blanks containing methanol and Cu(II), and recorded every 2 h after addition of Cu(II). In the experiment of GSH-driving releasing of copper, Cu(II)-induced UV/Vis absorption changes of **PL-I** in methanol /water (v/v, 1/1) were monitored before and after addition of GSH.

2.5. Cell culture

HepG2 cells were obtained from the shanghai Institute of Biochemistry and Cell Biology, Chinese Academy of Sciences, grown routinely in RPMI-1640 medium supplemented with 10% fetal bovine serum (FBS), 100 kU/L penicillin, and 100 kU/L streptomycin, and maintained 37 °C in a humidified atmosphere containing 5% CO_2.

2.6. Cell viability assay

HepG2 cells were seeded overnight in 10% FBS-containing RPMI-1640 at 5×10^3 cells in 96-well plates, then treated with graded concentrations of compounds or/and $CuSO_4{\cdot}5H_2O$ for 3 h, followed by their removal and incubation with fresh medium for another 45 h. After that, a fresh solution of MTT (0.5 mg/mL) was added to each well and the plate was incubated for another 4 h followed by the removal of the medium and the addition of 100 μL DMSO. The optical density (OD) of each well was read at 570 nm using a microplate reader (BIO-RAD model 550). The cell viability was expressed as the percentage of control.

2.7. Measurement of intracellular copper

An atomic absorption spectrophotometer (Varian AA-240) was used to determine the total copper content [29]. HepG2 cells (3×10^6 cells/dish) were seeded in 100 mm dishes. After 24 h, the cells were treated with 200 μM $CuSO_4{\cdot}5H_2O$ for 3 hour in the

presence of 15 μM **PL-I** or **PL**. Subsequently, the cells were incubated with fresh medium for 0.5 h and rapidly washed twice with ice-cold PBS to remove copper ions associated with the cell surface. Cells were collected and lysed in 2 mL 20% HNO_3 overnight at 4 °C for the determination of the total copper content using atomic absorption spectrometer. The results are expressed as folds of control values.

2.8. Fluorescence imaging of intracellular Cu(I)

Levels of Cu(I) in living HepG2 cells were imagined using a previously reported NIR fluorescent Cu(I) probe [26]. HepG2 cells seeded at a density of 1×10^5 cells/well in 6-well plates were treated with 15 μM **PL-I** in the presence or absence of 200 μM $CuSO_4\cdot5H_2O$ for 1, 2 or 3 h, followed by replacement of the medium with PBS and incubation of the Cu(I) probe (5 μM) for another 10 min at 37 °C. Subsequently, the cells were washed three times with PBS buffer. The fluorescence images were acquired by microscope Leica DM 4000B (Leica Microsystems CMS GmbH, Wetzlar, Germany) with a ×20 objective lens. In the case of inhibition, the cells were pretreated with BSO (400 μM) for 1 h before the test compounds were added.

2.9. Determination of intracellular ROS levels

ROS levels were detected by means of flow cytometry analysis with a redox-sensitive fluorescent probe DCFH-DA [30]. HepG2 cells were treated with 5, 10 and 15 μM **PL-I** for 3 h, in the presence and absence of 200 μM $CuSO_4\cdot5H_2O$ and incubated with fresh medium for another 3 h. After incubation, cells were collected and washed three times with PBS, then resuspended in PBS and incubated with 3 μM

DCFH-DA for 30 min at 37 °C. The DCF fluorescence was measured at 488 nm excitation and 525 nm emission using a FACSCanto flow cytometer (Becton-Dickinson, San Jose, CA, USA).

2.10. Assay for intracellular GSH and GSSG contents

The cyclic DTNB-GR assay [31] was used to monitor GSH and GSSG contents in HepG2 treated with the same fashion as described in determination of intracellular ROS levels, and the related details were provided in our previous paper [22].

2.11. Apoptosis and necrosis analysis

HepG2 cells were seeded in 6-well at 4×10^5 cells per well, and treated with different concentrations of **PL-I** or/and 200 μM $CuSO_4{\cdot}5H_2O$ for 3 h followed by their removal and incubation with fresh medium for another 45 h. After incubation, apoptosis and necrosis of cells were measured using a FACSCanto flow cytometer (Becton-Dickinson, SanJose, CA, USA) with an annexin V-FITC/PI apoptosis detection kit (BD Biosciences).

2.12. Statistical analysis

The data were expressed as the mean ± SD of the results obtained from at least three independent experiments. Significant differences ($P < 0.05$) between the means of two groups were analyzed by Student's t test.

3. Results and discussion

*3.1. Chemical synthesis of **PL-I** and Identification of its keto-enol structure*

PL-I was prepared in 89% yield from cyclopentanone by acylation with the freshly prepared acryloyl chloride in the presence of LDA in THF (Scheme 2). The proton

NMR spectrum of **PL-I** in DMSO-d_6 shows a broad singlet at δ 13.36 for its enolic hydrogen (Fig. 1). The peak areas for two *trans*-olefinic protons, which appeared as two sets of doublets at δ 7.58 and 6.96 with a coupling constant of 16.0 Hz, as well as δ 7.42 and 6.76 with a coupling constant of 15.6 Hz, respectively, allowed us to establish a ratio of the diketo to keto-enol forms in DMSO-d_6 being 1/10. Generally, DMSO reduces the enol concentration by hydrogen bonding with the enolic hydroxyl group, making this group less available for internal hydrogen bonding. However, the large proportion of the keto-enol form for **PL-I** was observed in DMSO due to the fact that the enolic double bond is in conjugation with the trimethoxycinnamyl group. Therefore, the trimethoxycinnamyl group would be an effective part contributing to the Cu(II) ionophoric property of **PL-I** (see below). It is known that the extent of enolization is greatly affected by solvent. This is also the case for the designed **PL-I** having a higher enol content in $CDCl_3$ (96%) than in DMSO (91%) (see NMR data in the Supporting information).

Notably, aside from the keto configuration (**PL-IA**), there are two possible enol configurations (**PL-IB** and **PL-IC**) for **PL-I** (Scheme 1). To specify the enol configuration, we calculated the geometries of the three isomers (**PL-IA**, **PL-IB** and **PL-IC**) of **PL-I** in the lowest energy conformation using Gaussian 09 program [28] (Fig. 2). A comparison of their relative Gibbs free energies shows clearly that **PL-IB** is the most thermodynamically stable, followed by **PL-IA**, whereas **PL-IC** is the least stable. Theoretical calculation of NMR parameters in $CDCl_3$ was further carried out to discriminate between the two possible enol isomers (**PL-IB** and **PL-IC**). It was found

that the calculated δ_C and δ_H values for **PL-IB**, compared with **PL-IC,** fit better with the experimental ones in $CDCl_3$ (see Table 1 and Fig. 3). Accordingly, the enol isomer of **PL-I** was specified as **PL-IB**.

*3.2. Cu(II)-induced UV/Vis absorption changes of **PL-I***

We assessed initially the Cu(II)-chelating property of **PL-I** by monitoring its UV/Vis absorption changes upon addition of Cu(II). From Fig. 4, it is evident that addition of Cu(II) to **PL-I** in methanol can induced promptly a decrease in its maximal absorption at 372 nm accompanied by the appearance of a bathochromic-shifted peak at 382 nm and a shoulder in the λ range of 325–350 nm (Line b). The new bands correspond to the formation of the Cu(II) complex with **PL-I** as supported by their intact return to initial 372 nm by EDTA, a well-known chelating agent (Line c). Importantly, the Cu(II) chelation with **PL-I** under acidic conditions was completely inhibited (Lines d and e), highlighting that the Cu(II) chelation depends on deprotonation of its enolic hydroxyl group. In contrast, the parent **PL** demonstrated no obvious chelation with Cu(II) even 10 h after addition (see the inset in Fig. 4) .

*3.3. Synergistic killing of HepG2 cells by the couple of **PL-I** and Cu(II)*

MTT colorimetric assay was subsequently performed to assay the cytotoxicity against human hepatoma HepG2 cells treated with the **PL-I** or/and cupric sulfate (100 or 200 μM) for ONLY 3 h followed by their removal and incubation with refresh medium for another 45 h (Fig. 5A). Under the current experimental conditions, neither **PL-I** nor Cu(II) alone (Data not shown) caused any obvious cytotoxicity, but

combination of the two induced concentration-dependent death of HepG2 cells. For example, in the presence of 200 μM Cu(II), the IC_{50} value of **PL-I** was 6.68 μM. It should be pointed out that 100 or 200 μM Cu(II) but significantly short treatment duration (3 h) were used in the above experiments. Therefore, Cu(II) should assist the effect at a much lower concentration matching conventional drug dosage standards by prolongation of treatment period, as suggested previously in the case of 3-HF as a potent Cu(II) ionophore [18]. In accordance with its inability to chelate Cu(II), the parent **PL** failed to exhibit this synergistic effect. Thus, the synergistic killing of HepG2 cells by the couple of **PL-I** and Cu(II) supports preliminarily that the designed **PL-I** can work as an ionophore transporting Cu(II) into the cells.

*3.4. Copper accumulation induced by the couple of **PL-I** and Cu(II)*

The ionophoric property of **PL-I** was further supported by assaying intracellular copper contents using Atomic Absorption Spectrometer. As shown in Fig. 5B, approximately 70-fold higher of copper accumulation was observed in HepG2 cells treated by the couple of **PL-I** and Cu(II) than the vehicle control. Moreover, the copper accumulation was also remarkably higher than those observed upon treatment with either **PL-I** or Cu(II) alone. In tune with its failure to exhibit synergic killing of HepG2 cells with Cu(II), the parent **PL** caused no obvious copper accumulation.

*3.5 GSH-driving intracellular releasing of Cu(I) from the Cu(II) complex with **PL-I***

GSH is the most abundant endogenous thiol with its concentration ranging from 1 to 15 mM depending on the cell types [32,33], also responsible for maintaining intracellular redox homeostasis [34]. We have previously proved that intracellular

dissociation of copper from **3-HF-Cu** is facilitated by GSH in a redox-responsive fashion [18]. To clarify whether GSH-driving releasing of copper is also the case for the Cu(II) complex with **PL-I**, Cu(II)-induced absorption changes of **PL-I** before and after addition of GSH were checked. When GSH was added, the bathochromic-shifted peak and shoulder corresponding to the formation of the Cu(II) complex with **PL-I** diminished and recovered almost to initial absorption spectrum of **PL-I** (Fig. 6A), Furthermore, addition of BCDS (a specific chelating agent for Cu(I)) in the system of **PL-I**, Cu(II) and GSH induced the appearance of a new band at 482 nm due to formation of the complex BCDS-Cu(I) (Fig. 6A and its inset). The above results support clearly dissociation of the Cu(II) complex with **PL-I** and releasing of Cu(I) by GSH.

To further clarify intracellular dissociation of the Cu(II) complex with **PL-I** by GSH, we used a NIR fluorescent Cu(I) probe [26] to image intracellular Cu(I) accumulation in living HepG2 cells. Neither Cu (II) nor **PL-I** alone demonstrated the ability to increase the red fluorescence (indicative of intracellular Cu(I) accumulation) (Fig. 7). However, their combination enhanced obviously the red fluorescence, and the signal intensity increased with increasing of incubation time. More importantly, the increased red fluorescence by the combination was abrogated by pretreatment of cells with BSO, a GSH synthase inhibitor. This provides a direct evidence for the intracellular dissociation of the Cu(II) complex with **PL-I** by GSH, and also for the ionophoric property of **PL-I**.

3.5. Redox imbalance, apoptosis and necrosis of HepG2 cells induced by the couple of

***PL-I** and Cu(II)*

The GSH-driving releasing of copper results in accumulation of Cu(I) and depletion of GSH, and thereby induces inevitably collapse of intracellular redox buffering system. This was evidenced by increase in the intracellular ROS levels (Fig. 8A) and decrease in the ratio of the reduced glutathione (GSH) to its disulfide (GSSG) (Fig. 8B), two important indicators of redox status. All these changes facilitate final apoptosis and necrosis of HepG2 cells by the couple of **PL-I** and Cu(II) (Fig.9). Noticeably, all the synergistic effects were observed by the couple in the related experiments including accumulation of Cu(I) (Figs. 5B and 7), redox imbalance (Fig. 8), as well as apoptosis and necrosis (Fig. 9) of HepG2 cells. The synergistic effects provide an entire evidence chain to support that by virtue of deprotonation of its enolic hydroxyl group, **PL-I** works as a potent Cu(II) ionophore to induce death of HepG2 cells in a redox intervention fashion.

Collectively, this work elucidates the importance and feasibility of a keto-enol moiety in developing natural product-inspired Cu(II) ionophores by the case of keto-enol-based modification on **PL**. As expected, the designed **PL-I** chelates effectively with Cu(II) in the enol form deprotonated to form a neutral and lipophilic complex able to pass through cellular membranes, followed by GSH-driving releasing of copper, resulting in accumulation of Cu(I), redox imbalance and final death of HepG2 cells (Scheme 3).

Acknowledgments

This work was supported by the National Natural Science Foundation of China

(Grant Nos. 21672091 and 21372109).

Appendix A. Supplementary material

Supplementary data associated with this article can be found in the online version at http://dx.doi.org/10.1016/j.freeradbiomed.

References

[1] B.E. Kim, T. Nevitt, D.J. Thiele, Mechanisms for copper acquisition, distribution and regulation, Nat. Chem. Biol. 4 (2008) 176-185.

[2] M.L. Turski, D.J. Thiele, New roles for copper metabolism in cell proliferation, signaling, and disease, J. Biol. Chem. 284 (2009) 717-721.

[3] E.I. Solomon, D.E. Heppner, E.M. Johnston, J.W. Ginsbach, J. Cirera, M. Qayyum, M.T. Kieber-Emmons, C.H. Kjaergaard, R.G. Hadt, L. Tian, Copper active sites in biology, Chem. Rev. 114 (2014) 3659-3853.

[4] F. Tisato, C. Marzano, M. Porchia, M. Pellei, C. Santini, Copper in diseases and treatments, and copper-based anticancer strategies, Med. Res. Rev. 30 (2010) 708-749.

[5] A. Gupte, R.J. Mumper, Elevated copper and oxidative stress in cancer cells as a target for cancer treatment, Cancer Treat. Rev. 35 (2009) 32-46.

[6] E.D. Harris, A requirement for copper in angiogenesis, Nutr. Rev. 62 (2004) 60-64.

[7] G.J. Brewer, Copper control as an antiangiogenic anticancer therapy: lessons from treating Wilson's disease, Exp. Biol. Med. 226 (2001) 665-673.

[8] D. Denoyer, S. Masaldan, S. La Fontaine, M.A. Cater, Targeting copper in cancer therapy: 'Copper That Cancer', Metallomics 7 (2015) 1459-1476 and references

therein.

[9] M.E. Helsel, K.J. Franz, Pharmacological activity of metal binding agents that alter copper bioavailability, Dalton Trans. 44 (2015) 8760-8770 and references therein.

[10] I. Alfonso, R. Quesada, Biological activity of synthetic ionophores: ion transporters as prospective drugs? Chem. Sci. 4 (2013) 3009-3019 and references therein.

[11] W.-Q. Ding, S.E. Lind, Metal ionophores-an emerging class of anticancer drugs, IUBMB Life 61 (2009) 1013-1018.

[12] J. Wang, C. Luo, C. Shan, Q. You, J. Lu, S. Elf, Y. Zhou, Y. Wen, J.L. Vinkenborg, J. Fan, H. Kang, R. Lin, D. Han, Y. Xie, J. Karpus, S. Chen, S. Ouyang, C. Luan, N. Zhang, H. Ding, M. Merkx, H. Liu, J. Chen, H. Jiang, C. He, Inhibition of human copper trafficking by a small molecule significantly attenuates cancer cell proliferation, Nat. Chem. 7 (2015) 968-979.

[13] S. Tardito, A. Barilli, I. Bassanetti, M. Tegoni, O. Bussolati, R. Franchi-Gazzola, C. Mucchino, L. Marchiò, Copper-dependent cytotoxicity of 8-hydroxyquinoline derivatives correlates with their hydrophobicity and goes not require caspase activation. J. Med. Chem. 55(2012) 10448-10459.

[14] M.A. Cater, H.B. Pearson, K. Wolyniec, P. Klaver, M. Bilandzic, B.M. Paterson, A.I. Bush, P.O. Humbert, S.L. Fontaine, P.S. Donnelly, Y. Haupt, Increasing intracellular bioavailable copper selectively targets prostate cancer cells, ACS Chem. Biol. 8(2013) 1621-1631.

[15] J.L. Allensworth, M.K. Evans, F. Bertucci, A.J. Aldrich, R.A. Festa, P. Finetti, N.T. Ueno, R. Safi, D.P. McDonnell, D.J. Thiele, S. Van Laere, G.R. Devi, Disulfiram (DSF) acts as a copper ionophore to induce copper-dependent oxidative stress and mediate anti-tumor efficacy in inflammatory breast cancer, Mol. Oncol. 9 (2015) 1155-1168.

[16] M. Nagai, N.H. Vo, L.S. Ogawa, D. Chimmanamada, T. Inoue, J. Chu, B.C. Beaudette-Zlatanova, R. Lu, R.K. Blackman, J. Barsoum, K. Koya, Y. Wada, The oncology drug elesclomol selectively transports copper to the mitochondria to induce oxidative stress in cancer cells, Free Radic. Biol. Med. 52 (2012) 2142-2150.

[17] S. Tardito, I. Bassanetti, C. Bignardi, L. Elviri, M. Tegoni, C. Mucchino, O. Bussolati, R. Franchi-Gazzola, L. Marchiò, Copper binding agents acting as copper ionophores lead to caspase inhibition and paraptotic cell death in human cancer cells, J. Am. Chem. Soc. 133 (2011) 6235-6242.

[18] F. Dai, W.-J. Yan, Y.-T. Du, X.-Z. Bao, X.-Z. Li, B. Zhou, Structural basis, chemical driving forces and biological implications of flavones as Cu(II) ionophores, Free Radic. Biol. Med. 108 (2017) 554-563.

[19] D.P. Bezerra, C. Pessoa, M.O. de Moraes, N. Saker-Neto, E.R. Silveira, L.V. Costa-Lotufo, Overview of the therapeutic potential of piplartine (piperlongumine), Eur. J. Pharm. Sci. 48 (2013) 453-463.

[20] L. Raj, T. Ide, A.U. Gurkar, M. Foley, M. Schenone, X. Li, N.J. Tolliday, T.R. Golub, S.A. Carr, A.F. Shamji, A.M. Stern, A. Mandinova, S.L. Schreiber, S.W.

Lee, Selective killing of cancer cells by a small molecule targeting the stress response to ROS, Nature 475 (2011) 231-234.

[21] W.-J. Yan, Q. Wang, C.-H. Yuan, F. Wang, Y. Ji, F. Dai, X.-L. Jin, B. Zhou, Designing piperlongumine-directed anticancer agents by an electrophilicity-based prooxidant strategy: A mechanistic investigation, *Free Radic. Biol. Med.* 97 (2016) 109-123.

[22] F. Dai, G.-Y. Liu, Y. Li. W.-J. Yan, Q. Wang, J. Yang, D.-L. Lu, D.-J. Ding, D. Lin, B. Zhou, Insights into the importance for designing curcumin-inspired anticancer agents by a prooxidant strategy: The case of diarylpentanoids, *Free Radic. Biol. Med.* 85 (2015) 127-137.

[23] Y. Li, L.-P. Zhang, F. Dai, W.-J. Yan, H.-B. Wang, Z.-S. Tu, B. Zhou, Hexamethoxylated monocarbonyl analogues of curcumin cause G2/M cell cycle arrest in NCI-H460 Cells via michael acceptor-dependent redox intervention, *J. Agric. Food Chem.* 63 (2015) 7731-7742.

[24] G.-J. Fan, X.-L. Jin, Y.-P. Qian, Q. Wang, R.-T. Yang, F. Dai, J.-J. Tang, Y.-J. Shang, L.-X. Cheng, J. Yang, B. Zhou, Hydroxycinnamic acids as DNA-cleaving agents in the presence of Cu^{II} Ions: Mechanism, structure-activity relationship, and biological implications, *Chem. Eur. J.* 15 (2009) 12889-12899.

[25] G.-Y. Liu, J. Yang, F. Dai, W.-J. Yan, Q. Wang, X.-Z. Li, D.-J. Ding, X.-Y. Cao, B. Zhou, Cu^{II} Ions and the stilbene-chroman hybrid with a catechol moiety synergistically induced DNA damage, and cell cycle arrest and apoptosis of

HepG2 cells: An interesting acid/base-promoted prooxidant reaction, *Chem. Eur. J.* 18 (2012) 11100-11106.

[26] X. Cao, W. Lin; W. Wan, Development of a near-infrared fluorescent probe for imaging of endogenous Cu^{+} in live cells. Chem. Commun. 48 (2012) 6247-6249.

[27] L.-D. Sun, F. Wang, F. Dai, Y.-H.Wang, D. Lin, B. Zhou, Development and mechanism investigation of a new piperlongumine derivative as a potent anti-inflammatory agent, Biochem. Pharmacol. 95 (2015) 156-169.

[28] M. J. Frisch, et al. Gaussian 09, Revision A.01, Gaussian, Wallingford, CT, 2009.

[29] X.-Q. Cai, N. Pan, G.-L. Zou, Copper-1, 10-phenanthroline-induced apoptosis in liver carcinoma Bel-7402 cells associates with copper overload, reactive oxygen species production, glutathione depletion and oxidative DNA damage, BioMetals 20 (2007) 1-11.

[30] R. Cathcart, E. Schwiers, B.N. Ames, Detection of picomole levels of hydroperoxides using a fluorescent dichlorofluorescein assay, Anal. Biochem. 134 (1983) 111-116.

[31] C. Vandeputte, I. Guizon, I. Genestie-Denis, B. Vannier, G. Lorenzon, A microtiter plate assay for total glutathione and glutathione disulfide contents in cultured/isolated cells: performance study of a new miniaturized protocol, Cell Biol. Toxicol. 10 (1994) 415-421.

[32] F. Yu, P. Li, P. Song, B. Wang, J. Zhao, K. Han, Facilitative functionalization of cyanine dye by an on–off–on fluorescent switch for imaging of H_2O_2 oxidative

stress and thiols reducing repair in cells and tissues, Chem. Commun. 48 (2012), 4980-4982.

[33] A. Pastore, F. Piemonte, M. Locatelli, A.L. Russo, L.M. Gaeta, G. Tozzi, G. Federici, Determination of Blood Total, Reduced, and Oxidized Glutathione in Pediatric Subjects, Clin. Chem. 47 (2001), 1467-1469.

[34] F.Q. Schafer, G.R. Buettner, Redox environment of the cell as viewed through the redox state of the glutathione disulfide/glutathione couple. Free Radic. Biol. Med. 30 (2001) 1191-1212.

Table 1 DFT-calculated and experimental chemical shifts (in ppm) for the two possible enol isomers (**PL-IB** and **PL-IC**) of **PL-I** in $CDCl_3$

	^{13}C NMR				^{1}H NMR		
	PL-I-B	**PL-I-C**			**PL-I-B**	**PL-I-C**	
	Cal.	Cal.	Exp.		Cal.	Cal.	Exp.
C-1	218.6	181.4	210.4	H-2	2.32	2.62	2.46
C-2	43.8	43.2	38.0	H-3	1.88	1.83	1.99
C-3	26.3	25.9	20.5	H-4	2.70	3.00	2.76
C-4	30.1	38.1	25.5	H-7	6.56	6.93	6.42
C-5	115.3	121.3	110.9	H-8	7.83	7.80	7.46
C-6	167.9	198.0	163.7	H-10	6.66	6.77	6.74
C-7	121.6	127.0	119.0	H-13	3.89	3.90	3.90
C-8	146.2	152.8	139.0	H-14	3.82	3.79	3.88
C-9	136.1	139.3	131.0				
C-10	106.1	112.5	105.0				
C-11	160.4	165.3	153.3				
C-12	145.2	151.2	139.5				
C-13	57.4	61.3	56.1				
C-14	62.8	66.1	61.0				

Scheme 1. (A) Proposed mechanisms of **3-HF** as a potent Cu(II) ionophore to induce death of HepG2 cells [18]; The dotted cycle shows its structural determinant (3-hydroxy-4-keto group) as a Cu(II) ionophore. (B) Designing a piperlongumine-inspired Cu(II) ionophore (**PL-I**) by introducing a keto-enol moiety as indicated by the dotted cycle.

Scheme 2. Synthesis of **PL-I**. Reagents and conditions: (a) $CH_2(COOH)_2$, Py, Piperidine, 95-100℃, 3 h; (b) $SOCl_2$, CH_2Cl_2, reflux, 4 h; (c) LDA/THF, -78 ^oC.

Scheme 3. Proposed mechanisms of **PL-I** as a potent Cu(II) ionophore to induce death of HepG2 cells.

Figure 1. ^1H NMR spectrum of **PL-I** in DMSO-d_6.

Figure 2. The DFT-calculated structures of the three isomers (**PL-IA**, **PL-IB** and **PL-IC**) of **PL-I** in the lowest energy conformation with their relative Gibbs free energies in parentheses.

Figure 3. Correlation analysis between the experimental and calculated chemical shifts (in ppm) of the two possible enol isomers of **PL-I** in $CDCl_3$. (A) and (C) for ^{13}C NMR of **PL-IB** and **PL-IC**, respectively; (B) and (D) for ^1H NMR of **PL-IB** and **PL-IC**, respectively.

Figure 4. Absorption spectral changes of **PL-I** (50 μM) in the absence and presence of 100 μM Cu(II) ions in methanol. a) **PL-I**; b) **PL-I** + Cu(II) c) **PL-I** + Cu(II) + EDTA (100 μM); d) **PL-I** + Cu(II) + H_2SO_4 (6.25 mM); e) **PL-I** + Cu(II) + H_2SO_4 (12.5 mM). The inset shows that there is no influence of addition of Cu(II) (100 μM) on absorption spectra of **PL** (50 μM, interval = 2 h).

Figure 5. (A) Dose-response cytotoxic curves in HepG2 cells treated with serial concentrations of **PL-I** or **PL** with and without 100 or 200 μM Cu(II) for only 3 h, and incubated with fresh medium for another 45 h. Data represent mean ± SD of three experiments. (B) Copper accumulation in HepG2 cells treated with **PL-I**, **PL** or/and Cu(II) at the indicated concentrations for 3 h. $^{**}P < 0.01$ versus the vehicle group.

Figure 6. Cu(II) (40 μM)-induced absorption changes of **PL-I** (40 μM) in methanol /water (v/v, 1/1) before and after addition of 2.8 mM GSH, followed by introduction of 40 μM BCDS. Inset shows absorption spectra of BCDS (40 μM) in the absence and

presence of Cu(I) (40 μM) in methanol /water (v/v, 1/1).

Figure 7. Fluorescence changes of the Cu(I) probe in living HepG2 cells treated with 15 μM **PL-I** in the presence or absence of 200 μM $CuSO_4 \cdot 5H_2O$ for 1, 2 or 3 h followed by incubation of the Cu(I) probe (5 μM) for another 10 min at 37 °C. When necessary, the cells were pretreated with BSO (400 μM) for 1 h before the tested compounds were added. Representative images are shown from three independent experiments.

Figure 8. ROS levels (A) and the ratios of GSH to its disulfide GSSG (B) in HepG2 cells treated with **PL-I** or/and Cu(II) at the indicated concentrations for 3 h, and incubated with fresh medium for another 3 h. $^{**}P < 0.01$ versus the vehicle group.

Figure 9. Flow cytometric analysis for apoptotic and necrotic induction of HepG2 cells treated with **PL-I** or/and Cu(II) at indicated concentrations for 3 h, and incubated with fresh medium for another 45 h. Percentage of cells in early and late apoptosis and necrosis is indicated in each quadrant.

Highlights

- Showing the significance of a keto-enol moiety for developing Cu(II) ionophores
- Keto-enol-based modification on piperlongumine to generate the designed PL-I
- Its keto-enol structure was well-identified by NMR and theoretical calculations
- This molecule in the enol form deprotonated can effectively complex Cu(II)
- This molecule triggers redox imbalance and death of HepG2 cells

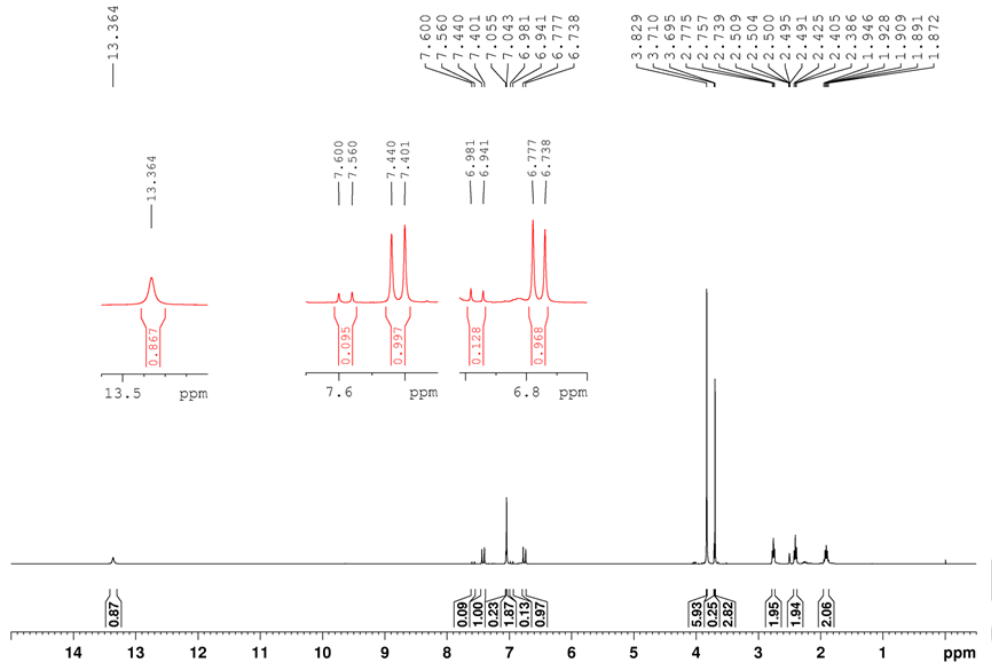

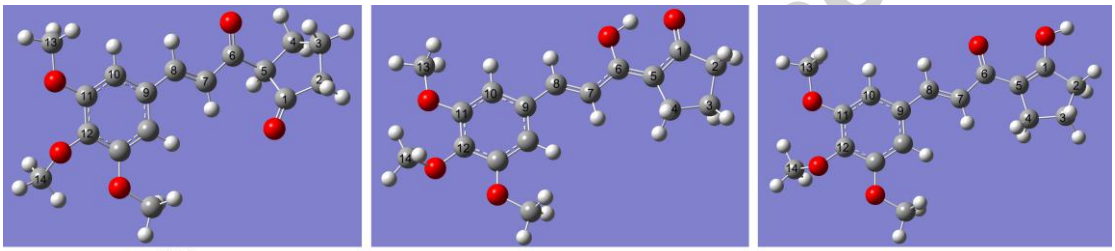

PL-I-A
(ΔG = 5.04 Kcal/mol)

PL-I-B
(ΔG = 0 Kcal/mol)

PL-I-C
(ΔG = 19.61 Kcal/mol)

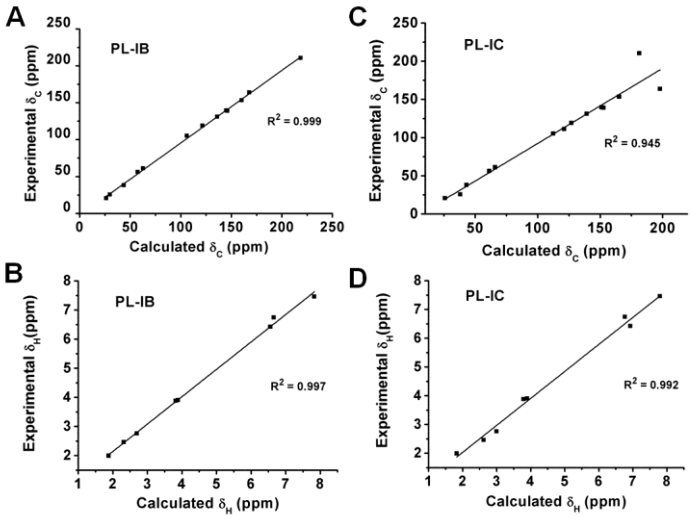

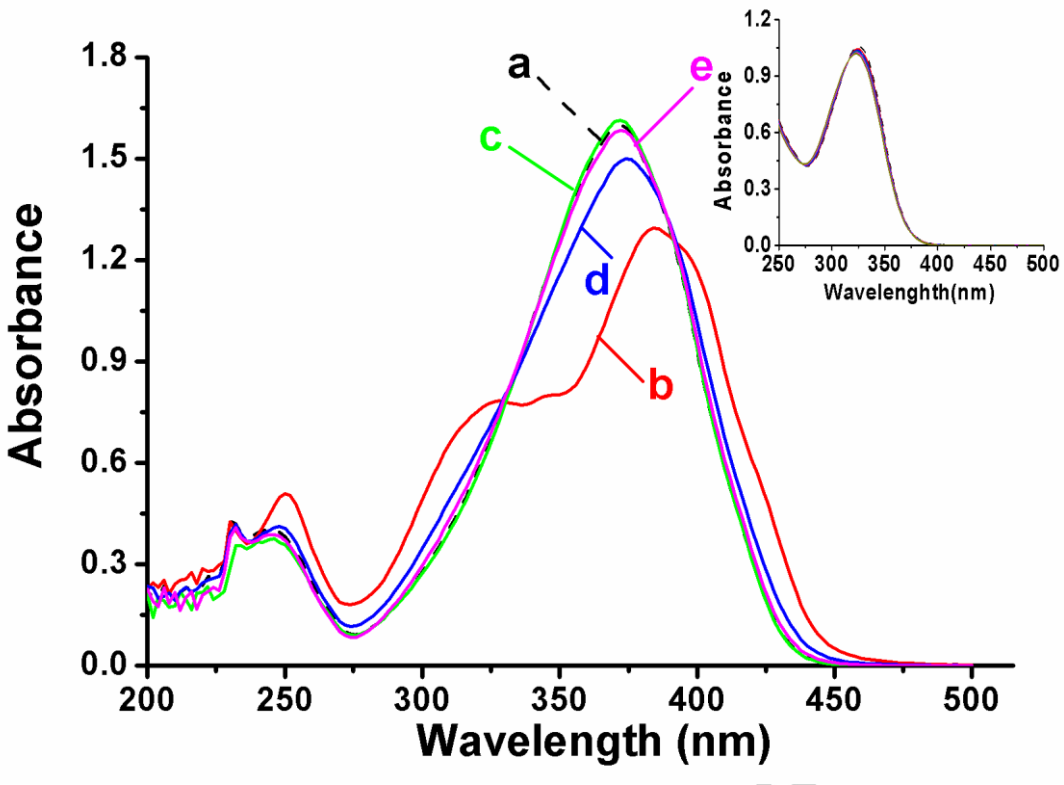

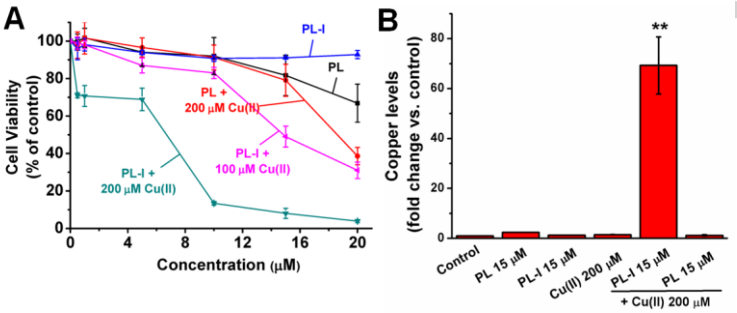

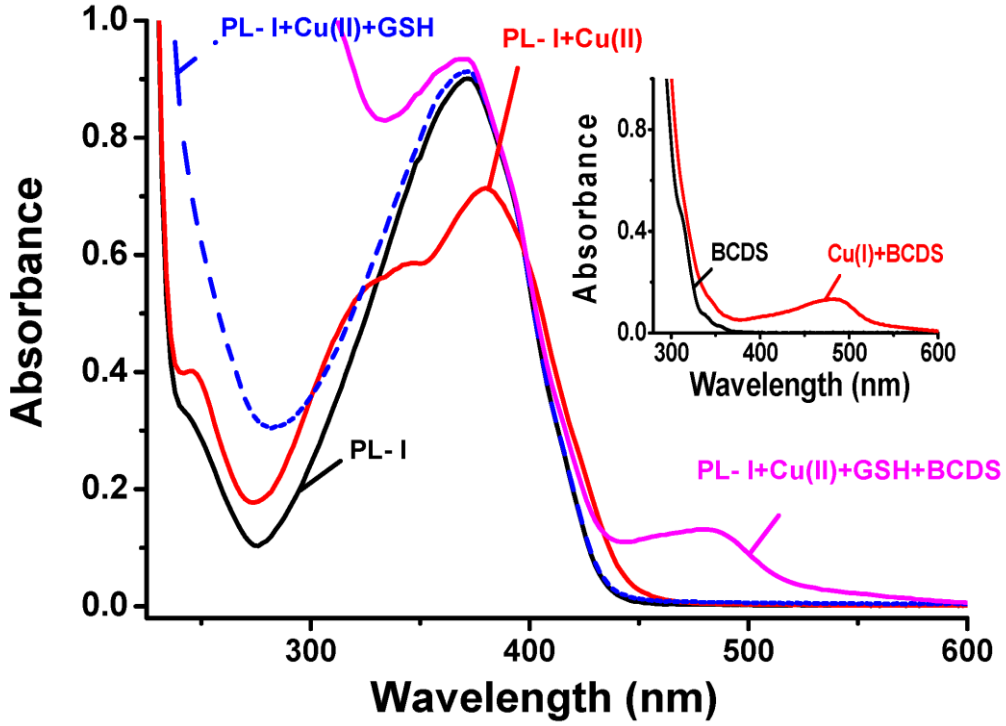
PL- I+Cu(II)+GSH
PL- I+Cu(II)
PL- I
PL- I+Cu(II)+GSH+BCDS
Absorbance
Wavelength (nm)
BCDS
Cu(I)+BCDS

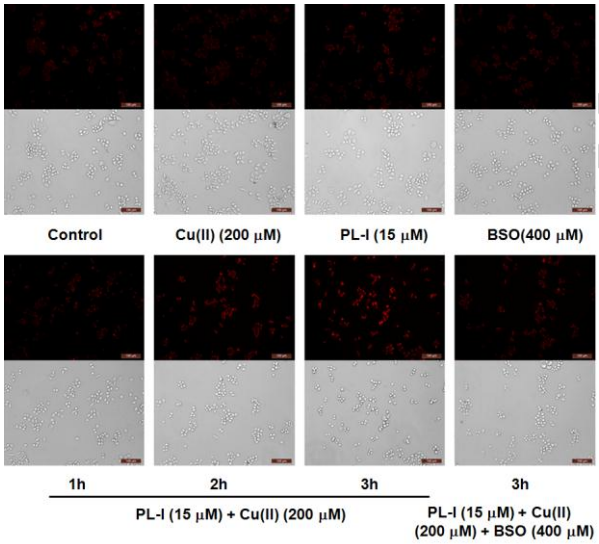
Control
Cu(II) (200 μM)
PL-I (15 μM)
BSO(400 μM)
1h
2h
3h
3h
PL-I (15 μM) + Cu(II) (200 μM)
PL-I (15 μM) + Cu(II) (200 μM) + BSO (400 μM)

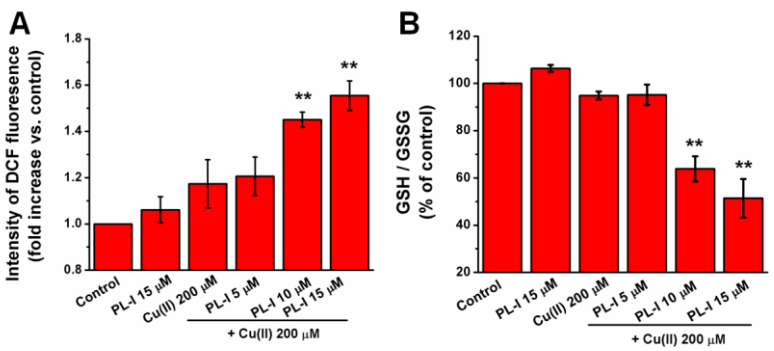
A
Intensity of DCF fluoresence (fold increase vs. control)
B
GSH / GSSG (% of control)
Control
PL-I 15 μM
Cu(II) 200 μM
PL-I 5 μM
PL-I 10 μM
PL-I 15 μM
+ Cu(II) 200 μM

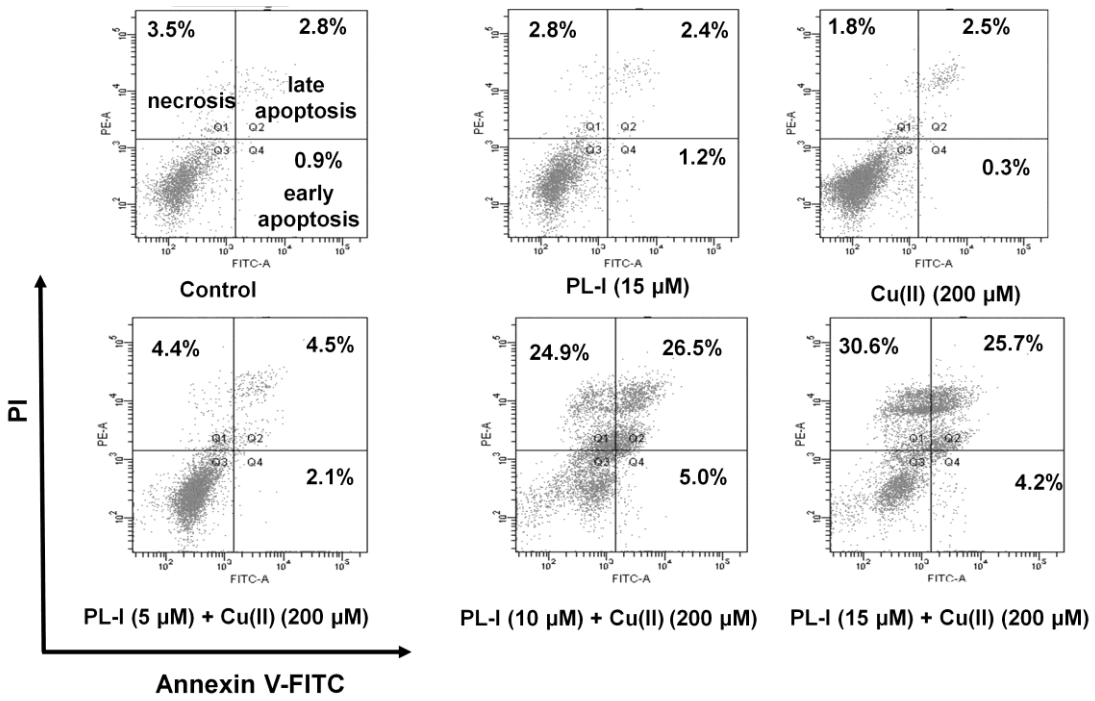
3.5%
2.8%
necrosis
late apoptosis
0.9%
early apoptosis
Control
2.8%
2.4%
1.2%
PL-I (15 μM)
1.8%
2.5%
0.3%
Cu(II) (200 μM)
4.4%
4.5%
2.1%
PL-I (5 μM) + Cu(II) (200 μM)
24.9%
26.5%
5.0%
PL-I (10 μM) + Cu(II) (200 μM)
30.6%
25.7%
4.2%
PL-I (15 μM) + Cu(II) (200 μM)
PI
Annexin V-FITC
PE-A
FITC-A
Q1
Q2
Q3
Q4

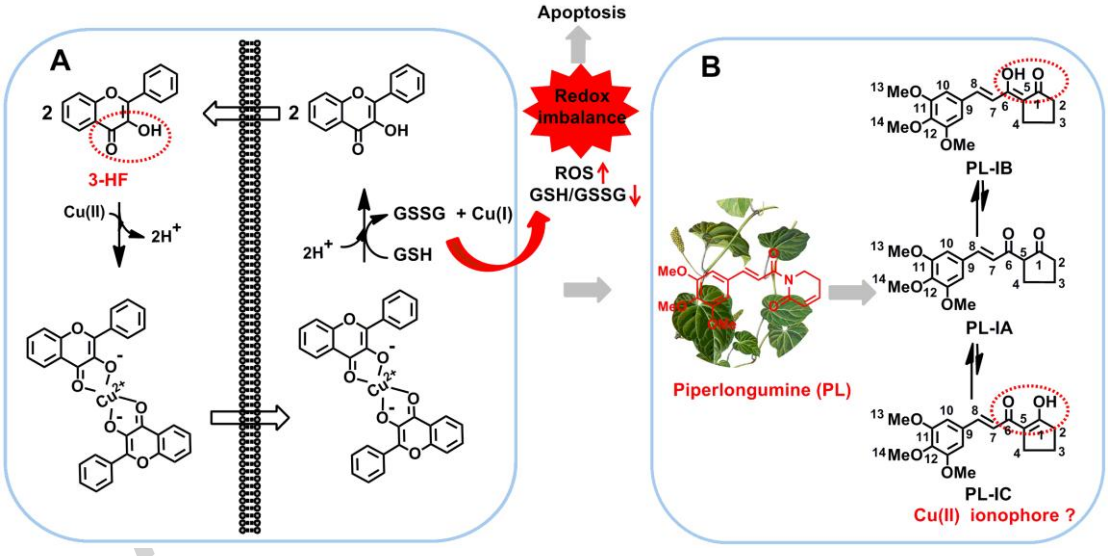
A
3-HF
Cu(II)
2H+
GSSG + Cu(I)
GSH
Apoptosis
Redox imbalance
ROS↑
GSH/GSSG↓
B
Piperlongumine (PL)
PL-IB
PL-IA
PL-IC
Cu(II) ionophore ?

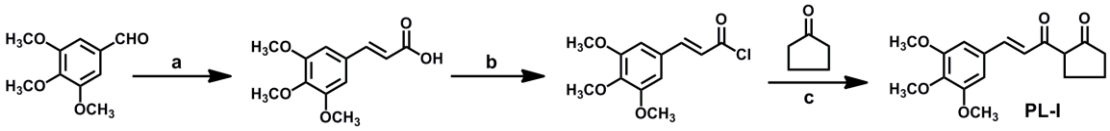
a
b
c
PL-I

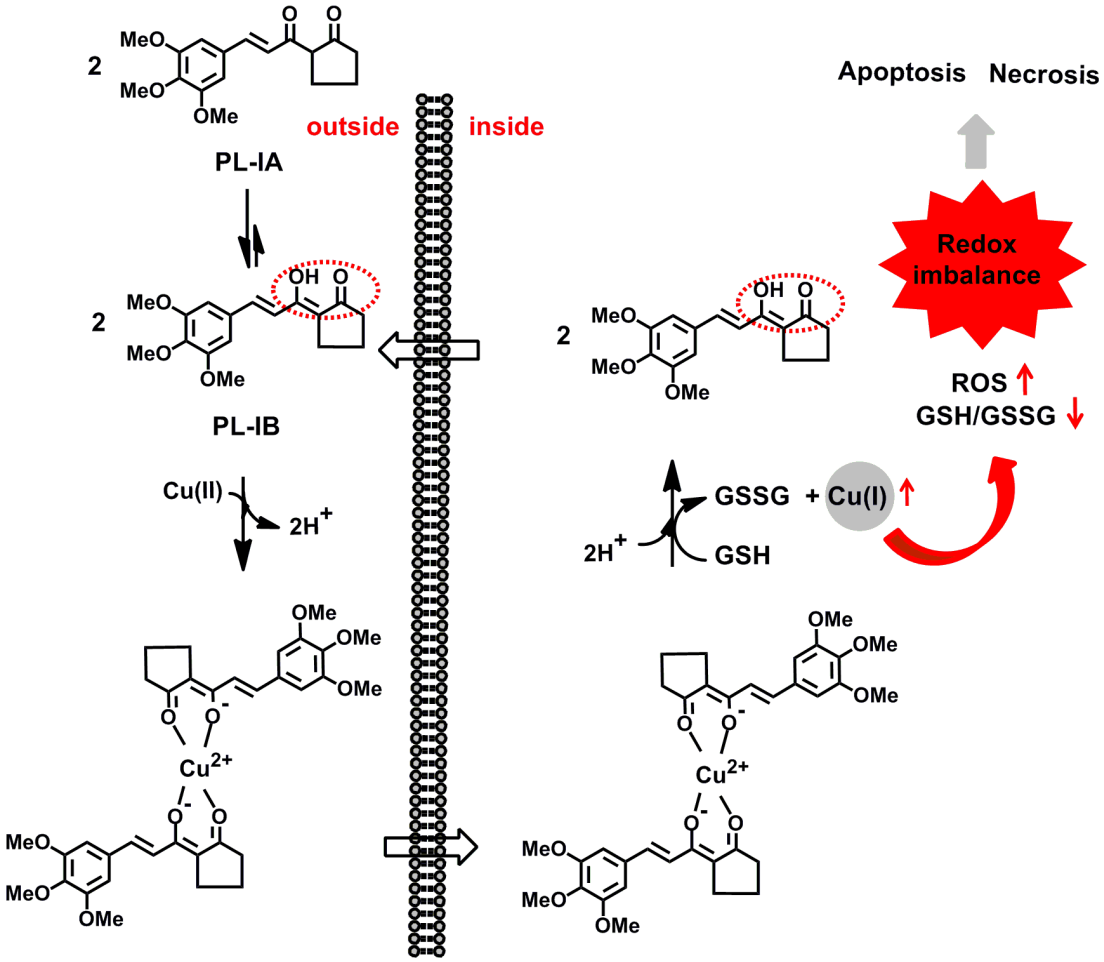
2
MeO
MeO
OMe
PL-IA
outside
inside
2
MeO
MeO
OMe
OH
O
PL-IB
Cu(II)
2H+
OMe
OMe
OMe
O
O-
Cu2+
O-
O
MeO
MeO
OMe
Apoptosis
Necrosis
Redox imbalance
2
MeO
MeO
OMe
OH
O
ROS ↑
GSH/GSSG ↓
2H+
GSSG
+ Cu(I) ↑
GSH
OMe
OMe
OMe
O
O-
Cu2+
O-
O
MeO
MeO
OMe